ACS Catalysis

Research Article

pubs.acs.org/acscatalysis

Characterization of the Surface Acidity of MFI Zeolite Nanosheets by ^{31}P NMR of Adsorbed Phosphine Oxides and Catalytic Cracking of Decalin

Yongbeom Seo, Kanghee Cho, Younjae Jung, and Ryong Ryoo*

Center for Nanomaterials and Chemical Reactions, Institute for Basic Science, and Department of Chemistry, KAIST, Daejeon 305-701, Republic of Korea

Supporting Information

ABSTRACT: MFI zeolite nanosheets tailored to 2.5-nm thickness were synthesized using a surfactant-type zeolite structure-directing agent, $[C_{22}H_{45}–N^+(CH_3)_2–C_6H_{12}–N^+(CH_3)_2–C_6H_{13}](Br^-)_2$. The zeolite nanosheets possessed Brønsted acid sites on their external surfaces as well as in the internal micropore walls. The acid strength and concentration was characterized by the ^{31}P NMR signals of the adsorbed trimethylphosphine oxide and tributylphosphine oxide. The ^{31}P NMR investigation identified three types of Brønsted acid sites with different strengths on external surfaces; there were four types inside the micropores. A linear correlation has been established between the number of the external strongest acid sites and the catalytic activity in decalin cracking for the MFI zeolite catalysts investigated in this work.

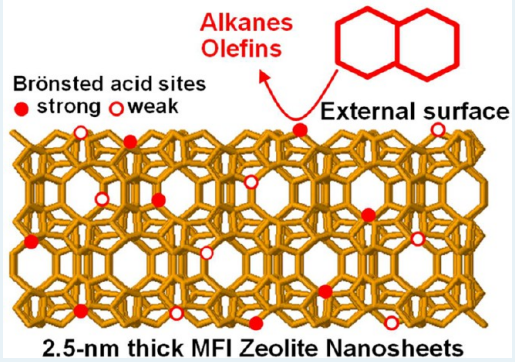

KEYWORDS: *acidity, zeolite nanosheets, NMR, phosphine oxide, cracking, decalin*

1. INTRODUCTION

Zeolites with crystalline microporous aluminosilicate frameworks are widely used as catalysts in petrochemical and oil refining processes and in fine chemical synthesis because of their strong acidity.[1−4] The acidity of zeolites originates from the structural Al atoms that are substituting for tetrahedral Si atoms and are coordinated to three or four oxygen atoms in the framework.[3,5] The tricoordinated Al site becomes a Lewis acid that can accept a pair of electrons from the adsorbed species. On the other hand, when the Al is tetracoordinated to oxygen, the framework becomes negatively charged. In this case, zeolites are synthesized with the framework charge compensated by the adsorption of Na^+ or ammonium ions under hydrothermal conditions. These cations can then be replaced by H^+ via ion exchange after synthesis. The exchanged H^+ ions can be located on the bridging oxygen between Si and Al, such as Si−OH^+−Al, becoming a Brønsted acid site. The acid strength varies according to the Si−O−Al angle and the presence of other framework Al atoms in the vicinity.[3] Both Lewis and Brønsted acid sites can catalyze various chemical reactions involving organic molecules. Conventional bulk zeolite catalysts are often used in the form of micrometer-sized crystallites either coated on a solid support or fabricated into pellets.[6] Despite the small crystal size, the external surface area of such conventional zeolites remains quite small as compared with the total surface area of the enormous number of internal micropores (<1 nm). Hence, chemical reactions taking place on external surfaces can be disregarded.

In recent years, there has been a great deal of interest in the catalytic properties of nanomorphic zeolite, that is, "a zeolite with a nanoscale morphology", such as nanoparticles,[7,8] nanosheets,[9] and mesoporous sponges.[10] Various methods of synthesis and postsynthetic treatments have been developed to obtain nanomorphic zeolites with very thin frameworks.[7−18] The framework thickness can be decreased even to a single-micropore level via layer-by-layer exfoliation techniques or synthesis routes using surfactants functionalized with zeolite structure-directing agents (SDA).[19] As the zeolite crystal thickness decreases to this level, the contribution of the external surfaces to the catalytic activity becomes significant. As an example of this, Corma et al. exfoliated a bulk MWW zeolite into monolayers.[20] The zeolite layers obtained in this manner exhibited high catalytic activity for benzene isopropylation to cumene. Roth et al. disintegrated a UTL zeolite into single layers of framework via a hydrolysis treatment.[21] In contrast, Ryoo et al. obtained nanosheets and mesoporous sponges with various types of zeolite frameworks via a synthesis route using zeolite-structure-directing surfactants.[9,10] The surfactant-directed MFI nanosheets exhibited remarkably enhanced lifetimes as a catalyst in methanol-to-hydrocarbon reactions, compared with the conventional MFI zeolite.[9] Moreover, MFI nanosheets and a beta zeolite nanosponge exhibited high catalytic activities in various reactions involving bulky molecules that were difficult to enter zeolite micropores.[10] Tsapatsis et al. also reported high catalytic performance of zeolite nanosheets in the liquid-phase mesitylene alkylation by benzyl

Received: December 18, 2012
Revised: February 27, 2013
Published: March 4, 2013

   dx.doi.org/10.1021/cs300824e | ACS Catal. 2013, 3, 713−720

alcohol.[22] As judged from these reactions with bulky molecules, such nanomorphic zeolites must possess acid sites on the external surfaces that could efficiently catalyze the reactions. However, little is known thus far about the acid strengths and concentrations of the surfactant-directed nanomorphic zeolites. More accurate information about the nature of the external acid sites would be valuable for an estimation of their catalytic properties for the development of catalytic applications.

Herein, we report the characterization of Brønsted acid sites that are located on external surfaces of the surfactant-directed (or -tailored) MFI zeolite nanosheets. To achieve this, we implemented the ^{31}P NMR spectroscopy analysis of adsorbed phosphine oxides. The ^{31}P NMR technique was originally developed using trialkylphosphine as the probe[23,24] and was later extended by several research groups using trialkylphosphine oxides.[25−27] Among various techniques to characterize zeolite acid sites (e.g., FT-IR,[28−31] NMR[23−27,32,33] and temperature-programmed desorption[34−36] of basic compounds), the ^{31}P NMR technique appears to be one of the most suitable techniques to provide quantitative analyses of acid sites located on the external surfaces of zeolite nanosheets.

Phosphine oxides are bases; therefore, molecules are strongly adsorbed on acid sites in the zeolite framework in a one-to-one manner.[25−27] The proton at the Brønsted acid site in a zeolite can interact with an oxygen atom from the phosphine oxide species (i.e., $H^+ \leftarrow O{=}PR_3$, where R indicates an alkyl group), resulting in a ^{31}P NMR chemical shift that increases according to the acid strength. NMR signals with different chemical shifts can be used for a quantitative analysis of acid sites with different acid strengths. Various phosphine oxides exhibiting different molecular sizes can be chosen to probe the internal or external surface acidity, depending on the molecular diameter in comparison with the zeolite pore apertures. In this work, we selected trimethylphosphine oxide (TMPO) and tributylphosphine oxide (TBPO). Because the kinetic diameter is 0.55 nm,[25] for TMPO, the phosphine oxide molecules can enter the apertures of MFI micropores (0.53 × 0.56 and 0.51 × 0.55 nm). Hence, the ^{31}P MAS NMR spectrum of the adsorbed TMPO can give information about the acid sites not only inside the MFI framework but also at the external surface. On the other hand, TBPO (~0.82 nm) is too bulky to enter the MFI zeolite micropore.[27] TBPO can be adsorbed exclusively on external surfaces for the titration of external acid sites. Hence, the adsorption difference between TMPO and TBPO corresponds to the acid sites present inside the zeolite nanosheets.

In recent years, there have been active studies to test MFI zeolite nanosheets as catalysts for liquid-phase reactions involving bulky molecules.[9,22] These studies confirmed the presence of catalytic active sites on external surfaces. However, the reactions were limited to esterification; Friedel−Crafts alkylation; and aldol condensation, which could be catalyzed by acid sites with moderate strength levels, such as those in the amorphous aluminosilicate frameworks of the mesoporous material Al-MCM-41.[37−39] Henceforth, a specific question regarding the acidity of the zeolite nanosheets was whether the external acid sites on the MFI nanosheets are sufficiently strong for hydrocarbon cracking. For this reason, we chose decalin cracking as a probe reaction. The decalin cracking reaction is known to require quite strong acid sites, such as those in USY and UTD-1 zeolites.[40,41] The molecular diameter of decalin is 0.7 × 0.52 nm[42] so that it is not likely to diffuse into the microporous channels of an MFI zeolite. Hence, it is very difficult for catalytic cracking of decalin to occur at any acid sites located inside the micropores.[40] These characteristics of decalin cracking make the reaction suitable as a probe to investigate the presence of strong acid sites on the external surfaces of MFI nanosheets.

2. EXPERIMENTAL SECTION

2.1. Materials Preparation. MFI zeolite samples were hydrothermally synthesized using a Teflon-lined stainless-steel autoclave at 150 °C in a laboratory, or it was received from Zeolyst. The synthesis process was performed with tetraethoxysilane (TEOS, TCI) as the silica source, and aluminum sulfate [$Al_2(SO_4)_3{\cdot}18H_2O$, Aldrich] as an alumina source. The Si/Al ratios of the starting mixtures were fixed at 20 in all cases. The zeolite products were filtered, washed with deionized water, and dried at 100 °C. The zeolites were then calcined in air for 4 h at 550 °C for the removal of organic SDAs. Subsequently, the zeolites were ion-exchanged into the NH_4^+ form three times in total using a 0.1 M aqueous solution of NH_4NO_3. The NH_4^+ form was converted to the H^+ form through calcination at 550 °C for 4 h. Further details of the zeolite synthesis conditions are briefly described as follows: tetrapropylammonium bromide (TPABr, Aldrich) was used as SDA for the synthesis of a conventional zeolite. The gel composition was 40 Na_2O/100 SiO_2/2.5 Al_2O_3/10 TPABr/26 H_2SO_4/9000 H_2O in molar ratios. The hydrothermal synthesis time was given for 5 d. To obtain a mesoporous zeolite sample, 5 mols of 3-[(trimethoxysilyl)propyl]hexadecyldimethylammonium chloride, was added as a mesopore-generating organosilane surfactant into the gel composition.[16] The remainder of the synthesis was identical to that used to prepare the conventional zeolite sample. A zeolite sample of 40-nm nanoparticles was synthesized using TPAOH (10 wt %, Aldrich) as SDA. The gel composition was 100 SiO_2/2.5 Al_2O_3/144 TPAOH/1920 H_2O/400 C_2H_5OH. The remainder of the synthesis procedure was identical to a method reported in the literature.[17] A sample of 2.5-nm-thick zeolite nanosheets was synthesized under the synthesis conditions used for the "multilamellar MFI" in Choi et al., using $[C_{22}H_{45}{-}N^+(CH_3)_2{-}C_6H_{12}{-}N^+(CH_3)_2{-}C_6H_{13}](Br^-)_2$ as SDA.[9] The gel composition was changed to 100 SiO_2/2.5 Al_2O_3/10 SDA/3 H_2SO_4/40 Na_2O/6000 H_2O for Si/Al = 20. To obtain a desilicated zeolite sample, a conventional ZSM-5 zeolite received from Zeolyst (CBV8014, NH_4 form, Si/Al = 42) was treated with a 0.2 M NaOH solution for 30 min at 60 °C under magnetic stirring as described in the literature.[29] An Al-MCM-41 sample was prepared via the postsynthetic incorporation of Al, following a procedure reported in the literature.[43] Both the desilicated zeolite and Al-MCM-41 sample were calcined at 550 °C and converted to the H^+ form after synthesis, in the same manner used with the synthesized zeolites.

2.2. Characterization. X-ray powder diffraction (XRD) patterns were recorded by a Rigaku Multiflex diffractometer using a monochromatized X-ray beam from Cu Kα radiation (40 kV, 30 mA). The XRD scanning was performed under ambient conditions at steps of 0.02, with an accumulation time of 0.5 s. For transmission electron microscopy (TEM), the powder sample was suspended in acetone by ultrasonication. A few droplets of suspended solutions were placed on a carbon microgrid, which was followed by drying under ambient conditions. TEM images were obtained with a Tecnai microscope operating at 300 kV (G2 F30) at room temperature. Nitrogen adsorption−desorption isotherms were measured at −196 °C using a volumetric gas sorption analyzer (Micromeritics TriStar II). Before the adsorption measurement, samples were outgassed for 3 h at 300 °C under 1 × 10^{-4} Pa. The Brunauer−

dx.doi.org/10.1021/cs300824e | ACS Catal. 2013, 3, 713−720

Table 1. Physicochemical Properties of the Materials

sample notation	description	ref	framework thickness/nm	Si/Al[a]	S_{BET}[b] /m^2 g^{-1}	S_{ext}[c] /m^2 g^{-1}	V_{micro}[d]/cm^3 g^{-1}	V_{tot}[e] /cm^3 g^{-1}
NS-2.5	MFI *nanosheet* by surfactant	9	2.5	22	550	400	0.070	0.57
OS-10	mesoporous MFI by *organosilane*	16	10−15	18	510	330	0.083	0.45
DZ-20	hierarchical MFI by *desilication*	29	15−25	26	460	260	0.092	0.41
NP-40	MFI *nanoparticle*	17	30−50	21	390	140	0.11	0.28
CB-300	*conventional* MFI *bulk* crystal	16	>300	20	330	90	0.11	0.15
Al-MCM-41	aluminosilicate *MCM-41*	43	∼1	18	930	840	0.020	1.31

[a]Si/Al mole ratio obtained from ICP/AES analysis. [b]S_{BET} is the specific BET surface area obtained from N_2 adsorption. [c]S_{ext} is the external surface area evaluated from the *t*-plot method. [e]V_{micro} is the micropore volume evaluated from the *t*-plot method. [d]V_{tot} is the total pore volume obtained at P/P_0 = 0.95.

Emmett−Teller (BET) equation was used to calculate the specific surface area from the adsorption branch in the region of P/P_0 = 0.05−0.30. The total pore volume was derived by the amount of N_2 adsorbed at P/P_0 = 0.95. The *t*-plot method was used to calculate the external surface area and micropore volume. The elemental analysis of the Si/Al ratios was confirmed by inductively coupled plasma atomic emission spectroscopy (ICP/AES) using an Optima 4300 DV instrument (Perkin-Elmer).

All NMR spectra were acquired in a solid state with magic angle spinning (MAS) using a Bruker Avance 400WB spectrometer at room temperature. ^{27}Al NMR spectra were obtained from fully hydrated zeolite samples at a frequency of 104.1 MHz using a single-pulse sequence at a spinning rate 12 kHz, a pulse width of 0.25 μs, and a recycle delay of 0.5 s. Hydrated $Al(NO_3)_3$ powder was used as an external reference. Before the ^{31}P MAS NMR measurements, samples were placed in a Pyrex cell equipped with a stopcock. The sample cell was outgassed at 300 °C. A methylene chloride solution containing a known amount of TMPO (100%, Alfa) or TBPO (98%, Acros) was added to the sample cell inside a glovebox to prevent moisture absorption. After mixing the solution and the sample well, the methylene chloride solvent was removed by evacuation at room temperature. The sample with phosphine oxide was transferred, inside a glovebox, into a NMR sample rotor that had a gastight cap. Then the ^{31}P MAS NMR spectrum was taken in a single-pulse sequence with a pulse width of 2 μs, a relaxation time of 5 s, and a spinning frequency of 12 kHz. Typically, 1200 (for TMPO) or 6000 (for TBPO) transients were accumulated to obtain spectra with an adequate signal-to-noise ratio. An aqueous 85% H_3PO_4 solution was used as an external reference to the chemical shift. A Gaussian deconvolution method was used to analyze the ^{31}P NMR spectrum. For the quantitative analysis of phosphine oxide adsorption on acid sites, the elemental analyses of Al, Si, and P were conducted by ICP/AES using a method described in the literature.[27]

2.3. Catalytic Measurements. The cracking of decalin was performed at 550 °C in a fixed-bed, fused-silica reactor equipped with a fritted disk (inside diameter = 13 mm), using 0.1 g of catalyst. Before the reaction started, the catalyst was activated at 550 °C for 2 h under an air flow (30 mL min^{-1}) in the reactor. Liquid decalin (TCI) was fed by a syringe pump at 0.12 mL min^{-1} into the upstream region of the reactor under a flow of high-purity N_2 at 60 mL min^{-1} (25 mol % decalin −75 mol % N_2). The weight hourly space velocity (WHSV) was maintained at 64.5 g g^{-1} h^{-1}. Decalin conversion was measured by a gas chromatograph equipped with a capillary column (GasPro, J&W Scientific). The conversion was recorded 5 min after starting the reactant flow for each sample.

3. RESULTS AND DISCUSSION

3.1. Tailoring the Zeolite Crystal Thickness. Five MFI zeolite samples with various crystal thicknesses and one Al-MCM-41 sample were prepared by following synthesis procedures reported in the literature.[9,16,17,29,39] The zeolite samples are denoted as CB-300, NP-40, DZ-20, OS-10, and NS-2.5, according to the preparation method and the mean crystal (or framework) thicknesses. The notation CB-300 denotes a "conventional bulk zeolite with particle diameter larger than 300 nm". The NP-40 zeolite indicates "nanoparticles with a thickness of 40 nm". The DZ-20 sample means a "desilicated zeolite with a framework thickness of 20 nm", as prepared through desilication of a conventional zeolite. The OS-10 sample means an "organosilane-directed mesoporous zeolite with a wall thickness of 10 nm". The NS-2.5 sample refers to MFI zeolite "nanosheets with a thickness of 2.5-nm". The "Al-MCM-41" sample indicates a "mesoporous MCM-41 material containing Al", which is composed of amorphous aluminosilicate pore walls. The Si/Al ratios, crystal thicknesses, BET surface areas, external surface areas, total pore volumes of these samples, and references to the synthesis methods are given in Table 1.

Figure 1A shows the XRD patterns of the zeolite samples obtained after calcination. All samples exhibited the characteristic Bragg reflections corresponding to a highly crystalline MFI zeolite structure. Figure 2 shows electron microscope images obtained from the calcined samples. The SEM images show that the CB-300 sample consisted of irregular particles larger than 300 nm in diameter. The NP-40 sample consisted of nanocrystals with a thickness of 30−50 nm. The DZ-20 sample showed irregular mesopores with diameters in the range of 10−15 nm. The mesopores were generated by the local dissolution of the bulk zeolite crystal. The remaining zeolite framework between adjacent mesopores ranged in thickness from 15 to 25 nm. The OS-10 zeolite exhibited nanosponge-like irregular mesoporous morphologies, which were composed of nanocrystalline frameworks that were 7−15 nm thick. The NS-2.5 sample was composed of MFI zeolite nanocrystals with the same 2.5-nm thickness along the crystal *b*-axis.

The present nanosheets were synthesized under the same synthesis conditions as those used for the multilamellar MFI reported previously, except for the Al content. In the previous report, the MFI nanosheets were synthesized in a pure silica form. The siliceous nanosheets were highly ordered in a layered manner and were supported by surfactant tails. The interlayer spacing in the siliceous MFI zeolite collapsed almost completely upon the removal of the surfactant through calcination. On the other hand, in the aluminosilicate NS-2.5 case here, the nanosheets were somewhat disordered and supported by each other. The mesopore volume in the interlayer region was retained even after calcination (0.50 cm^3 g^{-1}, the difference

dx.doi.org/10.1021/cs300824e | ACS Catal. 2013, 3, 713−720

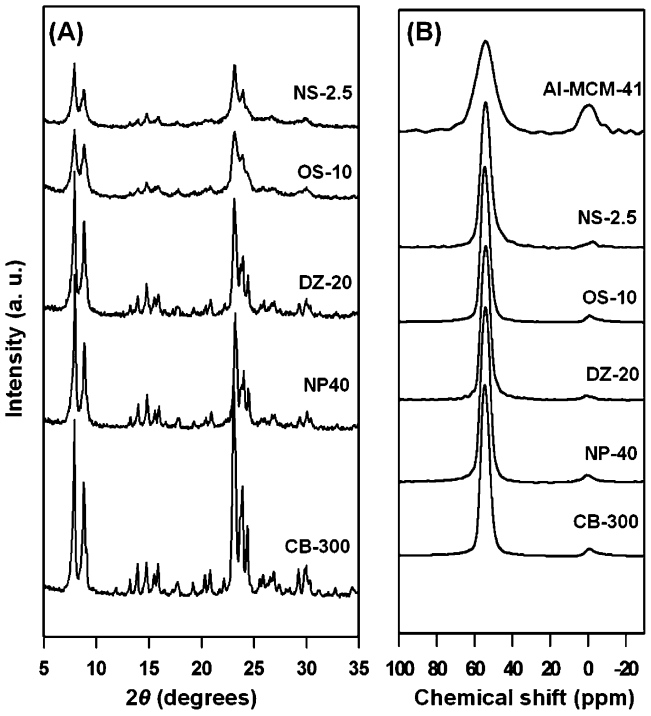

Figure 1. (A) Powder XRD patterns and (B) ^{27}Al MAS NMR spectra of calcined MFI zeolites prepared by various methods. For comparison, ^{27}Al MAS NMR spectrum of Al-MCM-41 is included in part B.

between the total pore volume and the micropore volume, as determined by N_2 adsorption). The distribution of the mesopore diameters exhibited a peak centered at 3.2 nm (Supporting Information Figure S1). The peak width was broader than the pore-size distribution of the pillared multilamellar MFI zeolite in Na et al.[44] but was nevertheless much narrower than the unilamellar MFI zeolite.[9] Regarding the interlamellar order and mesoporosity, the NS-2.5 sample in the present work was halfway between multilamellar and unilamellar. The decreased interlamellar ordering in NS-2.5 appeared to be due to the effect of the Al content in the synthesis composition. The crystal growth in the *ac* plane of the Al-containing nanosheets occurred more slowly as the Al content increased. The widths of the nanosheets decreased with an increase in the Al content. The narrow nanosheets in such a zeolite seemed easily tilted and irregularly packed.

The external surface area (S_{ext}) of the zeolite was determined following the *t*-plot method using N_2 adsorption isotherms. As the result in Table 1 shows, the S_{ext} values increased in the following order: CB-300 < NP-40 < DZ-20 < OS-10 < NS-2.5. This order is consistent with the decreasing order of the zeolite framework thickness. In this manner, we obtained a series of MFI zeolite samples in which the external surface area could vary over a sufficiently wide range for an investigation of the external surface acidity.

3.2. Total Acidity Probed by TMPO. The coordination state of Al in the MFI zeolite was checked by ^{27}Al MAS NMR spectroscopy. In all MFI zeolites investigated here, the NMR spectra exhibited two representative NMR peaks: 55 and 0 ppm (Figure 1B). The resonance peak at 55 ppm was very strong in terms of its intensity. This peak can be assigned to the Al species with the tetrahedrally coordinated framework. However, in the present single-pulse NMR measurements, the NMR peak cannot distinguish the Al locations between the internal micropores and the external surfaces. Compared with the tetrahedral Al signal, the NMR peak appearing at 0 ppm was very low in intensity. This peak is assignable to the octahedrally coordinated Al species, which can be present as an impurity in the synthesis or can be generated by dealumination from the framework during the high-temperature calcination. Compared with tetrahedral Al, the amount of the octahedral Al was very low in all zeolite samples. This result indicates that almost all Al atoms in the zeolite samples were located inside the zeolite frameworks, regardless of the preparation method or framework thickness. On the other hand, in the Al-MCM-41 sample, the NMR peak corresponding

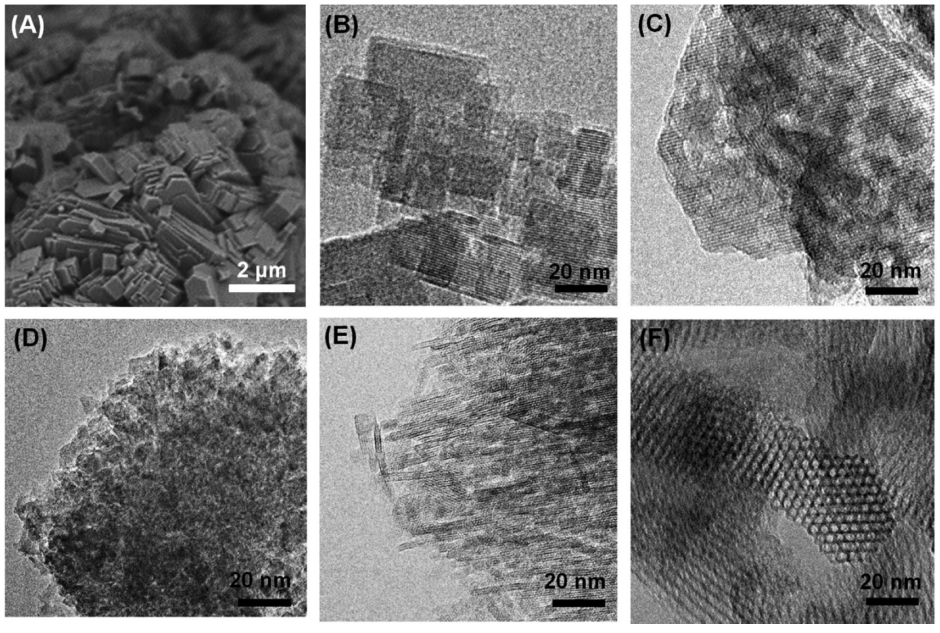

Figure 2. Electron microscope images of MFI zeolites: (A) SEM image of CB-300, and TEM images of (B) NP-40, (C) DZ-20, (D) OS-10, (E) NS-2.5, and (F) Al-MCM-41.

dx.doi.org/10.1021/cs300824e | *ACS Catal.* 2013, 3, 713−720

to the extra-framework Al was more intense. Another notable difference between the Al-MCM-41 sample (with an amorphous framework) and the crystalline zeolites was that the 55 ppm peak was relatively broad in the Al-MCM-41 case. This is consistent with the more disordered and less symmetric environments around Al in the case of the Al-MCM-41 sample.

Figure 3A shows the ^{31}P NMR spectra of TMPO as adsorbed on various MFI zeolites and the Al-MCM-41 sample. The NMR

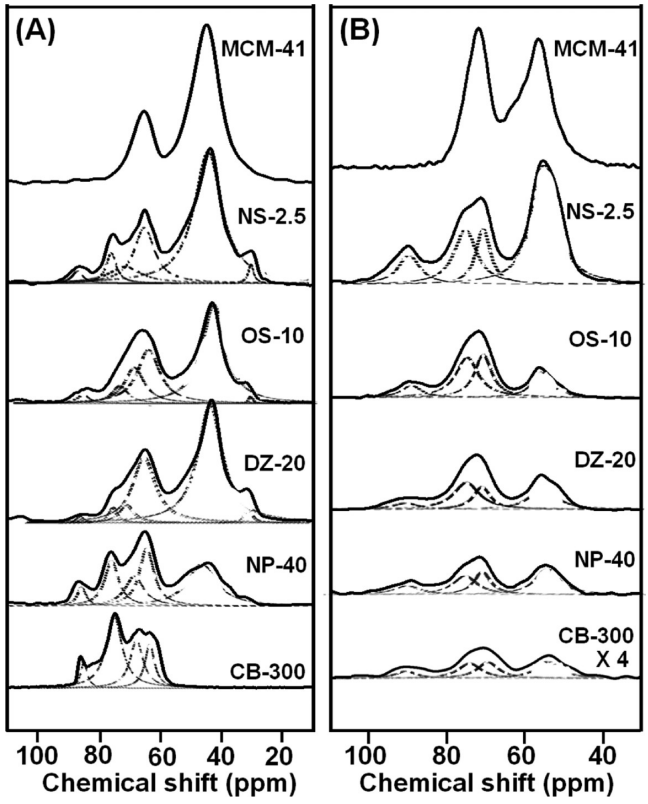

Figure 3. ^{31}P MAS NMR spectra of (A) TMPO and (B) TBPO adsorbed on the samples. The dotted curves indicate results of spectral analyses by Gaussian deconvolution. All spectra are plotted on the absolute intensity scale after collecting with the same number of acquisitions and being reduced to the same sample mass.

spectrum of the MFI zeolites could be deconvoluted by a Gaussian method into six peaks with chemical shifts of 30, 42, 66, 68, 76, and 86 ppm, respectively. Among these peaks, the NMR peak at 30 ppm can be assigned to the solid-state TMPO domain, which becomes present in the sample as it is physically separated from the zeolite phase if an excessively large amount of TMPO is loaded. Following the work of Zhao et al.,[27] the 42 ppm peak can be assigned to TMPO molecules that are weakly physisorbed on the zeolite surface or framework other than Brønsted acid sites. The other NMR peaks appearing at 66, 68, 76, and 86 ppm can be interpreted as resulting from the chemisorption of TMPO molecules on Brønsted acid sites.

The ^{31}P NMR chemical shift of phosphine oxide is known to increase according to the interaction strength with a Brønsted acid site and can therefore be used as an indicator of the acid strength. On the basis of the presence of four NMR peaks, the Brønsted acid sites in the MFI zeolite samples can be categorized into four groups with different acid strengths. They are denoted here as I, II, III, and IV. The acid group designated as "I" refers to the strongest acids, corresponding to the chemical shift of 86 ppm, and "II" indicates the second strong acid type causing the chemical shift of 76 ppm. The acid groups "III" and "IV" are weak acid sites, which correspond to the chemical shifts of 68 and 66 ppm, respectively. In all MFI zeolite samples, we confirmed the presence of I–IV acid groups.

The ^{31}P NMR peak area of adsorbed TMPO can be assumed to be proportional to the acid concentration of a given acid type if the NMR spectrum is taken with a sufficiently long relaxation delay time. The acid concentration can be calculated from the NMR peak area in combination with the elemental analyses of Al, Si, and P, following the procedure of Zhao et al. (see the Supporting Information).[27] Table 2 shows the concentrations of

Table 2. Classification and Concentration of Brønsted Acid Sites Probed by ^{31}P NMR of Adsorbed TMPO

	total acids titrated by TMPO				
acid group (^{31}P δ)	I (86[a])	II (76)	III (68)	IV (66)	A_{tot}[c]
NS-2.5	4.3[b]	12	22	17	56
OS-10	3.3	8.6	23	38	73
DZ-20	3.3	6.1	4.4	32	46
NP-40	4.2	16	14	23	57
CB-300	5.2	35	19	13	72

[a]The value indicates the chemical shift (δ) of adsorbed TMPO (ppm). [b]Values represent the partial concentration of acid sites ($\times 10^{-5}$ mol g^{-1}). [c]A_{tot} is the concentration of total acids ($\times 10^{-5}$ mol g^{-1}).

the four Brønsted acid groups (groups I–IV) obtained in this manner. The total acid concentration (A_{tot}) in Table 2 is the sum of these values. This concentration by TMPO includes both external surfaces and internal micropores.

Compared with the four Brønsted acid groups in the MFI zeolites, the Al-MCM-41 sample indicates only a single group of weak acids. The ^{31}P NMR spectrum of TMPO in the Al-MCM-41 sample shows two peaks: 45 and 66 ppm (Figure 3A). The 45 ppm peak can be assigned to the physisorption of TMPO, as in the case of MFI zeolites. On the other hand, the 66 ppm peak is attributed to the TMPO molecules chemisorbed on weak Brønsted acid sites. This peak is somewhat broad, but nevertheless difficult to deconvolute clearly. The broad peak indicates that there is a continuous distribution of acid strengths in this weak acid group. The ^{31}P NMR spectrum also indicates that the Al-MCM-41 mesoporous material does not possess strong acid sites. This result is in good agreement with the amorphous nature of the aluminosilicate framework.

3.3. External Acidity Probed by TBPO. When TBPO is used for the titration of Brønsted acid sites on a MFI zeolite instead of a TMPO, the phosphine oxide molecules are too bulky to enter the zeolite micropores. Hence, the phosphine oxide can exclusively detect the acid sites located on external surfaces. Figure 3B shows the ^{31}P NMR spectra obtained from TBPO. The NMR spectra can be deconvoluted using a Gaussian method, and the result can be interpreted in the same manner as in the case of TMPO. A notable difference between TBPO and TMPO is that the ^{31}P NMR chemical shift is greater in TBPO by approximately 6 ppm in the same chemical environment. For example, the TBPO in the solid state exhibits a chemical shift of 46 ppm, whereas the solid state TMPO shows a shift of 40 ppm. Taking into account the chemical shift difference, the three deconvoluted peaks appearing at 72, 74, and 92 ppm can be assigned to chemisorbed TBPO on Brønsted acid sites. A broad peak centered at 56 ppm can be assigned to weakly physisorbed TBPO on the external surface. This result indicates that the zeolite

dx.doi.org/10.1021/cs300824e | ACS Catal. 2013, 3, 713–720

nanosheets possess three types of Brønsted acid groups at the external surface, which can be designated as I, III, and IV. The acid sites corresponding to Group II appear to be missing from the external surfaces, regardless of the zeolite crystal thickness.

The concentration of the external acid sites was calculated from the TBPO NMR peak area, as in the case of TMPO. The external concentration is summarized in Table 3. This result shows that the fraction of the external acid sites among all Brønsted acid (i.e., A_{ex}/A_{tot}) increases very dramatically as the framework thickness decreases. The external fraction is only 5% in the case of the CB-300 bulk zeolite, but the fraction increases to 32% in the NS-2.5 zeolite nanosheets. The framework of the zeolite nanosheets can be represented by the structure model shown in Figure 4. According to this model, each nanosheet is composed of three pentasil layers. The external surface atoms, which are exposed to the upper and lower faces of a nanosheet, account for 33% of all framework atoms. This is very similar to the external fraction of Brønsted acid sites (i.e., A_{ex}/A_{tot} = 32%), as determined by TBPO ^{31}P NMR. These data indicate that there is no conspicuous difference in the local concentration of Brønsted acid sites between the external surfaces and internal micropores. Among the external acid sites (18×10^{-5} mol g^{-1}) of NS-2.5, 4.2×10^{-5} mol g^{-1} corresponds to the strong acids categorized as group I. The acid concentration belonging to group I on the external surfaces decreases in the following order: NS-2.5 > OS-10 > NP-40 > DZ-20 > CB-300, as shown in Table 3.

Table 3. Classification and Concentration of Brønsted Acid Sites Probed by ^{31}P NMR of Adsorbed TBPO

	external acids titrated by TBPO					
acid group (^{31}P δ)	I (92[a])	II (−)	III (74)	IV (72)	A_{ex}[c]	A_{ex}/A_{tot}[d]
NS-2.5	4.2[b]	N/A	5.3	8.4	18	32%
OS-10	2.3	N/A	7.2	9.2	19	26%
DZ-20	1.4	N/A	5.6	4.2	11	23%
NP-40	1.6	N/A	3.6	2.6	7.8	14%
CB-300	0.6	N/A	1.4	1.4	3.4	4.7%

[a]The value indicates the chemical shift (δ) of adsorbed TBPO (ppm). [b]Values represent the partial concentration of external acid sites ($\times 10^{-5}$ mol g^{-1}). [c]A_{ex} is the concentration of total external acids ($\times 10^{-5}$ mol g^{-1}). [d]A_{ex}/A_{tot} is the molar ratio of the external acids to total acids.

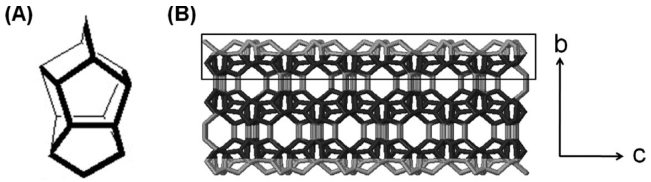

Figure 4. Schematic representations of (A) a pentasil unit, and (B) the b−c plane of NS-2.5. The rectangle in part (B) indicates the pentasil sheet, and the light gray region in the rectangle marks the external part of NS-2.5.

3.4. External Acidity vs Decalin Cracking. Decalin cracking was performed at 550 °C under the same conditions for all catalyst samples, using the same amounts of catalyst. The reaction conditions were chosen such that the maximum conversion of decalin would be less than 20% for any sample. Under such a low conversion rate, the reactant concentration in a catalyst bed can be approximated as constant when deriving the rate equation. The measured conversion rate under this condition becomes approximately proportional to the turnover rate. In Figure 5, the decalin conversion measured with each catalyst sample is plotted in terms of the external surface concentration of the strong Brønsted acid sites belonging to Group I. This result shows that the Al-MCM-41 sample has no significantly measurable concentration of such strong acid sites, and accordingly, the catalytic conversion was almost negligible (0.4%). On the other hand, the CB-300, DZ-20, NP-40, OS-10, and NS-2.5 MFI zeolite samples contain progressively increasing amounts of the strong acid sites on the external surface. These samples exhibit high catalytic conversions in proportion to the strong acid concentrations. That is, there is an excellent linear correlation between the conversion of decalin and the external acid concentration assigned to group I. The reaction temperature was lowered to 500 °C to check the possibility of hydrogen transfer.[45] At this temperature, the decalin conversion was very low, as compared with 550 °C (6% even with the nanosheet catalyst). The result confirmed a good linear correlation between the catalytic conversion and the strong acid concentration. This result indicates that the Brønsted acid sites belonging to group I on the external surfaces are the catalytic active centers for decalin cracking. The acid sites belonging to groups III and IV appear to be too low in strength to carry out the cracking reaction under the given reaction conditions. If we include these weak acid sites, the correlation in Figure 5 fails to exhibit a linear correlation any longer.

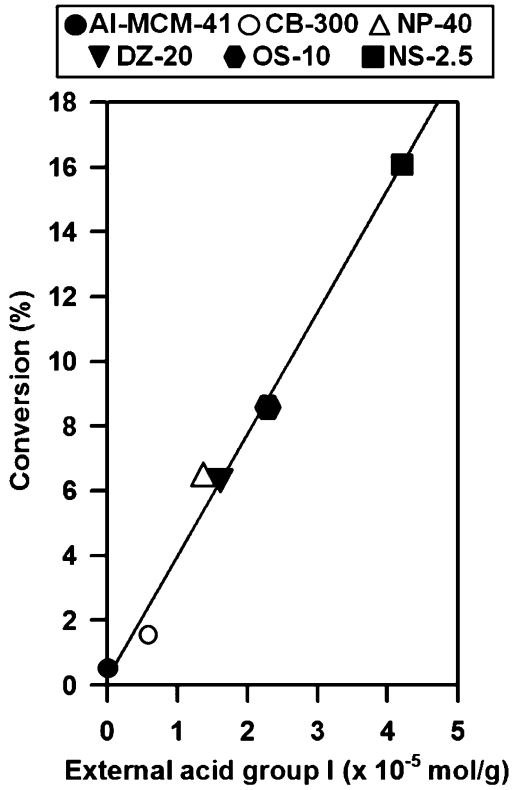

Figure 5. The conversion in decalin cracking plotted versus the concentration of group I external acid sites (reaction conditions: WHSV of decalin = 64.5 g g^{-1} h^{-1}, catalysts 0.1g, and temperature 550 °C). The turnover frequency of the NS-2.5 catalyst becomes 0.12 s^{-1} if it is calculated by the concentration of group I acid sites.

The catalytic activity of the MFI zeolite nanosheets is even comparable to those of other large-pore zeolites into which

dx.doi.org/10.1021/cs300824e | ACS Catal. 2013, 3, 713−720

decalin can enter for cracking. For this comparison, we tested commercial samples of zeolite beta (ZEOcat PB/H, Si/Al = 12.5) and USY zeolite (TOSOH HSZ-360HUA, Si/Al = 7.5). These zeolites were converted to the H^+-ionic forms through NH_4^+ ion exchange and calcination in the same manner as used for the MFI zeolite samples. The catalytic conversion was measured under the same reaction conditions described above and using the same catalyst weight. The beta zeolite treated in this manner exhibited a decalin conversion rate of 78% and a USY value of 80%. Compared with these values, the 16% decalin conversion by the present MFI nanosheets appears to be quite low. Nevertheless, regarding the very low Al content in the MFI nanosheets and the low external surface fraction, the decalin cracking to this conversion is considerable. The product selectivity was compared after adjusting the conversion of each zeolite to about 16% by changing the amount of catalyst. The MFI zeolite nanosheet exhibited higher selectivity for short chain olefins (C_2~C_4) than the large pore zeolites (Supporting Information Table S1). The higher selectivity of the short-chain olefins is attributed to the higher probability of secondary reactions, such as dealkylation and cracking in smaller micropore channels, followed by ring-opening of decalin.[40]

4. CONCLUSIONS

The acidity of a MFI zeolite nanosheet with a thickness of 2.5 nm was successfully characterized using ^{31}P MAS NMR with adsorbed trimethylphosphine oxide and tributylphosphine oxide. The ^{31}P NMR investigation revealed that the MFI zeolite nanosheet possessed 5.6×10^{-4} mol of Brønsted acid sites per gram of sample. These acid sites correspond to 77% of the total Al content (Si/Al = 22). Among the total Brønsted acid sites, 1.8×10^{-4} mol was located on the external surfaces. Among the external acid sites, 4.2×10^{-5} mol (5.8% of the total Al content) corresponded to "strong acid" sites. Owing to the strong acids on the external surfaces, the MFI zeolite nanosheet exhibited very high catalytic activity in terms of decalin cracking as compared with a conventional MFI zeolite. Therefore, it is expected that these nanosheets and, perhaps, related nanomorphic zeolites that can be tailor-synthesized by dual (both micro and meso levels) structure-directing surfactants would be useful in a wide range of acid-catalyzed reactions involving bulky species.

■ ASSOCIATED CONTENT

Supporting Information

Calculation details for acid sites; nitrogen adsorption–desorption isotherm and pore size distribution for MFI nanosheets; additional catalytic data. This material is available free of charge via the Internet at http://pubs.acs.org.

■ AUTHOR INFORMATION

Corresponding Author

*Phone: (+82) 42-350-2830. Fax: (+82) 42-350-8130. E-mail: rryoo@kaist.ac.kr.

Notes

The authors declare no competing financial interest.

■ ACKNOWLEDGMENTS

This work was supported by the Research Center Program (CA1201) of IBS (Institute for Basic Science) in Korea. Solid state NMR studies were performed at the research analysis center at KAIST. Y. Seo wishes to thank Prof. F. Kleitz (Laval University, Canada) for the scientific discussion.

■ REFERENCES

(1) Corma, A. *Chem. Rev.* **1997**, *97*, 2373–2419.
(2) Cundy, C. S.; Cox, P. A. *Chem. Rev.* **2005**, *82*, 1–78.
(3) Corma, A. *Chem. Rev.* **1995**, *95*, 559–614.
(4) Rinaldi, R.; Schüuth, F. *Energy Environ. Sci.* **2009**, *2*, 610–626.
(5) Ward, J. W. *Zeolite Chemistry and Catalysis*. American Chemical Society: Washington, DC, 1976, p 118
(6) Corma, A.; Gracia, H. *Chem. Rev.* **2003**, *103*, 4307–4365.
(7) Li, Q.; Creaser, D.; Sterte, J. *Microporous Mesoporous Mater.* **1999**, *31*, 141–150.
(8) Tosheva, L.; Valtchev, V. P. *Chem. Mater.* **2005**, *17*, 2494–2513.
(9) Choi, M.; Na, K.; Kim, J.; Sakamoto, Y.; Terasaki, O.; Ryoo, R. *Nature* **2009**, *461*, 246–249.
(10) Na, K.; Jo, C.; Kim, J.; Cho, K.; Jung, J.; Seo, Y.; Messinger, R. J.; Chmelka, B. F.; Ryoo, R. *Science* **2011**, *333*, 328–332.
(11) Groen, J. C.; Bach, T.; Ziese, U.; Donk, A. M. P.; de Jong, K. P.; Moulijn, J. A.; Pérez-Ramírez, J. *J. Am. Chem. Soc.* **2005**, *127*, 10792–10793.
(12) Jacobsen, C. J. H.; Madsen, C.; Houzvicka, J.; Schmidt, I.; Carlsson, A. *J. Am. Chem. Soc.* **2000**, *122*, 7116–7117.
(13) Holland, B. T.; Abrams, L.; Stein, A. *J. Am. Chem. Soc.* **1999**, *121*, 4308–3409.
(14) Yang, Z.; Xia, Y.; Mokaya, R. *Adv. Mater.* **2004**, *16*, 727–732.
(15) Schmidt, I.; Boisen, A.; Gustavsson, E.; Ståhl, K.; Pehrson, S.; Dahl, S.; Carlsson, A.; Jacobsen, C. J. H. *Chem. Mater.* **2001**, *13*, 4416–4418.
(16) Choi, M.; Cho, H. S.; Srivastava, R.; Venkatesan, C.; Choi, D.-H.; Ryoo, R. *Nat. Mater.* **2006**, *5*, 718–723.
(17) Müller, M.; Harvey, G.; Prins, R. *Microporous Mesoporous Mater.* **2000**, *34*, 135–147.
(18) Ogura, M.; Shinomiya, S.-Y.; Tateno, J.; Nara, Y.; Kikuchi, E.; Matsukata, M. *Chem. Lett.* **2000**, *29*, 882–883.
(19) Jung, J.; Jo, C.; Cho, K.; Ryoo, R. *J. Mater. Chem.* **2012**, *22*, 4637–4640.
(20) Corma, A.; Martínez-Soria, V.; Schnoeveld, E. *J. Catal.* **2000**, *192*, 163–173.
(21) Roth, W. J.; Shvets, O. V.; Shamzhy, M.; Chlubná, P.; Kubů, M.; Nachtigall, P.; Čejka, J. *J. Am. Chem. Soc.* **2011**, *133*, 6130–6133.
(22) Zhang, X.; Liu, D.; Xu, D.; Asahina, S.; Cychosz, K. A.; Agrawal, K. V.; Wahedi, Y. A.; Bhan, A.; Hashimi, S. A.; Teraskai, O.; Thommes, M.; Tsapatsis, M. *Science* **2012**, *336*, 1684–1687.
(23) Lunsford, J. H.; Rothwell, W. P.; Shen, W. *J. Am. Chem. Soc.* **1985**, *107*, 1540–1547.
(24) Baltusis, L.; Frye, J. S.; Maciel, G. E. *J. Am. Chem. Soc.* **1986**, *108*, 7119–7120.
(25) Rakiewicz, E. F.; Peters, A. W.; Wormsbecher, R. F.; Sutovich, K. J.; Mueller, K. T. *J. Phys. Chem. B* **1998**, *102*, 2890–2896.
(26) Osegovic, J. P.; Drago, R. S. *J. Phys. Chem. B* **2000**, *104*, 147–154.
(27) Zhao, Q.; Chen, W.-H.; Huang, S.-J.; Wu, Y.-C.; Lee, H.-K.; Liu, S.-B. *J. Phys. Chem. B* **2002**, *106*, 4462–4469.
(28) van Donk, S.; Bus, E.; Broersma, A.; Bitter, J. H.; de Jong, K. P. *J. Catal.* **2002**, *212*, 86–93.
(29) Thibault-Starzyk, F.; Stan, I.; Abelló, S.; Bonilla, A.; Thomas, K.; Fernandez, C.; Gilson, J.-P.; Pérez-Ramírez, J. J. *Catal.* **2009**, *264*, 11–14.
(30) Busca, G. *Chem. Rev.* **2007**, *107*, 5366–5410.
(31) Gil, B.; Zones, S. I.; Hwang, S. J.; Bejblova, M.; Čejka, J. *J. Phys. Chem. C* **2008**, *112*, 2997–3007.
(32) Pfeifer, H.; Freude, D.; Hunger, M. *Zeolites* **1985**, *5*, 274–286.
(33) Farcasiu, D.; Leu, R.; Corma, A. *J. Phys. Chem. B* **2002**, *106*, 928–932.
(34) Topsoe, N. Y.; Pedersen, K.; Derouane, E. G. *J. Catal.* **1981**, *70*, 41–52.
(35) Farneth, W. E.; Gorte, R. J. *Chem. Rev.* **1995**, *95*, 615–635.
(36) Suzuki, K.; Aoyagi, Y.; Katada, N.; Choi, M.; Ryoo, R.; Niwa, M. *Catal. Today* **2008**, *132*, 38–45.
(37) Carmo, A. C.; de Souza, L. K. C.; da Costa, C. E. F.; Longo, E.; Zamian, J. R.; da Rocha Filho, G. N. *Fuel* **2009**, *88*, 461–468.

(38) Bhattacharyya, K. G.; Talukdar, A. K.; Das, P.; Sivasanker, S. *J. Mol. Catal. A: Chem.* **2003**, *197*, 255−262.
(39) Iwanami, K.; Sakakura, T.; Yasuda, H. *Catal. Commun.* **2009**, *10*, 1990−1994.
(40) Corma, A.; González-Alfaro, V.; Orchillés, A. V. *J. Catal.* **2001**, *200*, 34−44.
(41) Kubička, D.; Kumar, N.; Mäki-arvela, P.; Tiitta, M.; Niemi, V.; Salmi, T.; Murzin, D. Y. *J. Catal.* **2004**, *222*, 65−79.
(42) Singleton, N. L.; Huddersman, K. D.; Needham, M. I. *J. Chem. Soc., Faraday Trans.* **1998**, *94*, 3777−3780.
(43) Jun, S.; Ryoo, R. *J. Catal.* **2000**, *195*, 237−243.
(44) Na, K.; Choi, M.; Park, W.; Sakamoto, Y.; Terasaki, O.; Ryoo, R. *J. Am. Chem. Soc.* **2010**, *132*, 4169−4177.
(45) Lukyanov, D. B.; Shtral, V. I.; Khadzhiev, S. N. *J. Catal.* **1994**, *146*, 87−92.